Oxidation behaviour of ultrafast slurry aluminized nickel

Thomas Kepa, Gilles Bonnet, Fernando Pedraza

Oxidation behaviour of ultrafast slurry aluminized nickel

Thomas Kepa[a,*], Gilles Bonnet[a], Fernando Pedraza[a,*]

[a]Laboratoire des Sciences de l'Ingénieur pour l'Environnement, Université de La Rochelle, LaSIE UMR-CNRS 7356, Avenue Michel Crépeau, 17042 La Rochelle Cedex 1, France

*Corresponding authors: thomas.kepa1@univ-lr.fr (T. Kepa), fpedraza@univ-lr.fr (F. Pedraza)

Abstract :

The isothermal oxidation behaviour of ultrafast slurry aluminized pure nickel was studied between 900 and 1100°C in air for 100h. The microstructure and composition of the coatings evolved with the increase of the oxidation temperature resulting in a progressive reduction of aluminium content of the initial bilayered Ni_2Al_3 + NiAl coating. The oxidation curves exhibited a parabolic shape due to the formation of α-Al_2O_3 scale. The parabolic rate constants increased from 950 to 1100°C in line with the faster degradation of the coating. Moreover, the kinetic constant at 900°C was higher than at 950°C because of a greater formation of the less protective metastable θ-Al_2O_3 scale developed rather than α-Al_2O_3. While the oxidation kinetics of the ultrafast slurry coatings are one order of magnitude higher than that of pack-cemented coatings, the evolution of the microstructure is alike to the ones of slowly grown CVD-derived and slurry aluminide coatings.

Keywords: High temperature oxidation; Isothermal oxidation; Slurry aluminizing; Coating; Nickel.

1 Introduction

Aluminide coatings are employed in different fields of application like power plants and aeronautical engines to improve the resistance of critical components to high temperature oxidation and corrosion. Indeed, the good mechanical and protective properties of these coatings are well recognized [1, 2]. Processes like CVD [3, 4], pack cementation [5, 6] or hot dipping [7, 8] are commonly employed to elaborate aluminium diffusion coatings. In CVD and pack cementation, aluminizing occurs by adsorption of an Al-containing gas precursor molecule, which is then hydrolysed or reduced. The Al atoms finally incorporate into the bulk by solid-state diffusion. For these processes, both the microstructure and the composition are controlled by the activity of the aluminium (high or low activity coatings), i.e. the amount of Al precursors supplied to the surface of the substrate and the temperature [9, 10].

Similar Al-diffusion coatings can be achieved by slurry [11] that often involves the appearance of molten Al and the dissolution of the metal substrate resulting in self-propagating high-temperature synthesis (SHS) reactions and a subsequent solid-state diffusion once any of the reagents has been consumed [12]. The slurries are usually composed of organic binders and contain phosphorus and Cr(VI) derivatives [11, 13]. In contrast, Pedraza et al. employed additive-free water-based slurries to obtain high activity aluminide coatings on pure Ni [14, 15] and on different Ni-based superalloys [16] similar to those elaborated by other diffusion coating processes.

However, like with CVD-like techniques, the slurry coating processes often require several steps comprising many hours of diffusion treatments at different temperatures. In an attempt to obtain aluminide coatings in a faster manner, Bauer et al. studied a “fast aluminizing” slurry process of a Ni-rich Fe-based alloy [17] that necessarily modified the microstructures of the

coating because of the short dwell times (3 to 5 min) at temperatures between 700 and 1000°C. The different methods (induction, heating mat and burner) were carried out under air (no protective gas) and led to the oxidation of Al particles during the process and to heterogeneous coatings. While the feasibility of fast aluminizing was clearly demonstrated in Bauer's work, neither the control of the aluminizing process nor the oxidation resistance and the stability of the coating were considered. Therefore, our previous study on "fast slurry aluminizing" under argon atmosphere investigated the formation of homogenous coarse-grained (~50 µm) coatings of NiAl (Al rich) on pure nickel similar to those obtained by pack cementation [18]. However, neither the high temperature oxidation resistance nor the potential evolution of the microstructure of these fastly-grown coatings with temperature were elucidated, which is the main aim of this work.

Indeed, when aluminide coatings are exposed to high temperatures, the formation of a protective α-Al_2O_3 scale from the coating may be compromised with the consumption of the Al reservoir [19]. In this view, Mollard et al. thoroughly investigated the evolution of conventional (slowly-grown) high activity slurry coatings with temperature on the formation of the allotropic varieties of alumina and spinel ($NiAl_2O_4$) oxides and compared the results with similar coatings obtained by pack cementation [20]. The parabolic rate constants were slightly higher than those obtained for the pack cemented coatings because their microstructure and composition of the slurry coatings evolved more rapidly with temperature, resulting in the formation of the $NiAl_2O_4$ spinel in addition to α-Al_2O_3. In contrast, the pack cemented coatings never grew the spinel oxide. Similar results were obtained after the isothermal oxidation at 1100°C of the slowly-grown slurry Al-coated Rene N5 Ni-based superalloy [21]. After 100h, the parabolic rate constant of slurry coating was again somewhat greater than that of the out-of-pack aluminide coating due to the fast evolution of the high activity slurry coating compared to that of the low activity out-of-pack and the derived formation of thicker duplex α-Al_2O_3/ $NiAl_2O_4$.

Galetz et al. also reported a rapid evolution of the high activity slurry Al coating on Alloy 602CA when isothermally oxidized for 100h between 900 and 1200°C due to the significant Al gradient between the top of their coatings and the substrate [22]. The greater evolution and kinetics of the slowly-grown slurry aluminide coatings than the pack cemented or out-of-pack ones can result from the small grain size of the former, allowing faster transport of Al to form the oxide and diffusion into the substrate [23].

Since the grain size in the fast-slurry aluminide coatings is as coarse as the pack cemented ones (~50 μm) it is assumed that they should provide better oxidation resistance at high temperatures than the slowly-grown slurry aluminides. Indeed, the fast-aluminized slurry coatings are believed to be off-thermodynamic equilibrium. This is because the ultrafast slurry process involves self-propagating high temperature synthesis (SHS) reactions between molten Al and solid Ni inducing a quite significant local raise in temperature to produce a melt in just a few seconds [24]. The very short aluminizing times (~35 min) [18] may not allow to dissipate the heat flux of the exothermic reactions, hence introducing metallurgical defects (vacancies, dislocations, voids…) like in welding processes involving the appearance of molten metal. Off-equilibrium aluminide coatings do not necessarily behave worse than conventional pack cemented diffusion coatings as demonstrated by Shen et al. for their Ni_2Al_3/NiAl coatings using low energy Al-radiation [25]. The authors attributed the sole formation of α-Al_2O_3 to the surface nanostructuring and bulk nanocavities formed upon irradiation that fostered the flow of Al. According to previous SHS studies of NiAl [24, 26, 27], the resulting Ni_xAl_y phases should not be nanostructured. In contrast, the natural content of vacancies in the Ni_xAl_y intermetallics [28] should be increased due to the rapid quench after the strong exothermic SHS melting.

Therefore, this work intends to unveil the oxidation behaviour of the very-fast slurry aluminide coatings under synthetic air between 900 and 1100°C for 100h. A special emphasis is put on the analysis of the microstructural and chemical evolution of the coatings to establish a direct

comparison with slowly-grown aluminide coatings (pack cementation and slurry routes) [20] and ascertain the stability of these new fast aluminized coatings.

2 Experimental

Pure nickel samples (Goodfellow, 99.9 % purity) of 12.7 mm of diameter and an approximate thickness of 1.5 mm were ground with SiC P180 paper, rinsed with deionized water, then with ethanol (3 minutes in an ultrasonic bath), and finally dried in hot air before the deposition of the slurry by spraying.

The slurry was composed of 43 wt.% aluminium microparticles (Hermillon, 99.9 % purity, 2-5 µm average size) mixed in 57 wt.% of an aqueous binder (PVA/water with a mass ratio 1/10). Each surface was sprayed with 12 ± 1 $mg \cdot cm^{-2}$ of slurry and allowed to dry in ambient air for at least 1h.

The consecutive heat treatment was conducted in a thermobalance (SETARAM TGA 92) under argon flow (20 $mL \cdot min^{-1}$) for a very short time, contrary to that required to elaborate coatings by "classical" slurry route for which the overall processing time exceeded 12h [14, 29, 30]. The fast heat treatment consisted in a quick heating ramp (at 100°C/min) from room temperature till 1080°C, followed by a dwell time of 5 min and, finally, a rapid quench at 50°C/min to keep the high temperature microstructure, composition and phases of the coatings. Overall, the coating process duration was about 35 minutes. The residue of the slurry left over the aluminized surface was sand-blasted with alumina (mesh 220) in a SANDMASTER FG-94 apparatus prior to the oxidation tests.

The isothermal oxidation tests were performed in a SETARAM TGA SETSYS 1750 thermobalance (10^{-7} g accuracy). The apparatus was first purged from air by a vacuum pump. Inert argon gas was then flowed (20 $mL \cdot min^{-1}$) all along the heating ramp (50°C·min^{-1}) up to the oxidation temperature where the gaseous atmosphere was switched to flowing (16 $mL \cdot min^{-1}$) synthetic air (80 vol.% N_2 - 20 vol.% O_2). At the end of the oxidation experiments, the samples were cooled down at a rate of 50°C/min. The time and oxidation temperatures were

identical to the ones employed by Mollard et al. [20] to allow direct comparison. Thus, the isothermal oxidations were conducted from 900 to 1100°C (every 50°C) in synthetic air for 100 hours.

The crystalline phases of the coatings were determined before and after oxidation by X-Ray Diffraction (XRD) using a Bruker AXS D8 Advance set-up (Cu K_α radiation, λ= 0.15418 nm) in the θ-2θ mode, from 10 to 90°. The samples surfaces were also analysed after oxidation by Raman spectroscopy with a Jobin Yvon High Resolution (LabRaman HR) using a He-Ne laser, combined to an optical microscope (Olympus BX 41) and a CCD detector. In order to protect the outermost part of the oxide scale from spalling during metallographic preparation, the samples were gold coated (plasma coater Cressington Sputter coater 108 auto) and then nickel electroplated (Watts bath). The cross-sections were observed before and after etching (Kalling n°2 etchant: $CuCl_2$, HCl, ethanol) under a FEI Quanta 200F scanning-electron microscope (SEM). The chemical analyses were conducted with the EDAX detector with a Si drift detector (SDD) coupled to the SEM using EDAX GENESIS software.

3 Results and discussion

3.1 As aluminized nickel samples

Figure 1.a shows the SEM cross-section of the sample in the as-coated condition. A diffusion coating of about 60 µm thick and composed of two major distinctive layers grew after 5 min at 1080°C (heating ramp of 100°C/min). The outermost part of the coating corresponds to the Ni_2Al_3 phase according to the EDS profile plotted in figure 1.b and the XRD patterns (Fig. 2) and is about 35 µm thick. It can be observed that this layer contains some submicron cavities located within the grains and at the grain boundaries, possibly related to the fast shrinkage of the melt upon cooling and accumulation of vacancies. The second major layer is about 25 µm thick and is attributed to NiAl according to the EDS analysis but this cannot be assessed by XRD because of the insufficient penetration depth of the X-rays. Between the main coating and the substrate, two very thin layers (55 to 60 µm deep) can also be observed likely corresponding to the NiAl (Ni rich) and γ'-Ni_3Al, according to the EDS spot analyses (not shown).

Our previous work using the same fast aluminizing treatment on pure nickel [18] demonstrated the sole formation of hyperstoichiometric NiAl phase and no Ni_2Al_3 nor Ni_3Al. The reason for this is related to the lower amount of slurry deposited (10 $mg \cdot cm^{-2}$) than in the present work (12 $mg \cdot cm^{-2}$), hence supplying more Al to the coating upon the same aluminizing time. In contrast, the overall thickness (~60 µm) is quite similar to the one obtained with either the fast aluminizing (10 $mg \cdot cm^{-2}$) [18], or the slowly grown (5°C/min) slurry coatings including two isothermal stages (700°C/2h + 1100°C/2h [14, 30]), or the one obtained by pack cementation in the work of Mollard et al. [20]. The aluminium content is however lower with pack cementation and long-time slurry processes because of the promotion of outward diffusion of nickel with time at high temperature. This would imply that the thickness of the coatings is controlled by the main intermetallic phase (NiAl) given its very large composition range [31].

After aluminizing, the topcoat corresponding to the oxidized shell of the emptied Al microparticles (bisque) [20] was removed by light sand-blasting and then analysed by XRD before the isothermal tests. All the X-ray patterns exhibited the Ni_2Al_3 peaks (Figure 2) but with different relative intensities attributed to the variability of the deposited mass (12 ± 1 $mg \cdot cm^{-2}$).

3.2 Isothermal oxidation tests

3.2.1 Kinetics

Figure 3.a shows the mass gain per surface unit (ΔM/S) against time of the fast-aluminized nickel oxidized in air at different temperatures for 100h. The specific mass gain increases with the oxidation temperature, except for the coated sample oxidized at 900°C for which the mass gain is higher than those registered at 950 and 1000°C. Several authors reported a similar behaviour on alumina forming bulk materials like β-NiAl + Zr [32], pure NiAl [33], (Ni, Pt)Al [34], and FeCrAl alloys [35], or on Al microparticles [36, 37] or slurry aluminides [17]. The higher mass gain for 900°C can be attributed to the preferential formation of metastable θ-Al_2O_3 (rather than α-alumina) growing at this temperature by the presence of twin boundaries and the intrinsic cation vacancy network allowing faster diffusion than in the nearly close packed structure (i.e. α-Al_2O_3) [35]. Otherwise, all the curves display a parabolic shape and the parabolic constants (k_p) calculated from the $(\Delta M/S)^2$ curves against oxidation time (fig 3.b) are gathered in Table 1.

Table 1: Parabolic rate constants for nickel samples coated either by fast slurry aluminizing (no residues, this work), "Particoat" (slow treatment with residues) slurry process [20], by pack cementation and by Particoat (slow treatment) without the foam (residues) on top [38].

Temperature (°C)	k_p ($g^2.cm^{-4}.s^{-1}$)			
	Present work (fast)	**Particoat[20] (slow)**	**Pack cementation[20] (slow)**	**Particoat without foam[38] (slow)**
900	1.5×10^{-13}	7.7×10^{-14}	1.5×10^{-13}	-
950	3.7×10^{-14}	1.3×10^{-12}	6.3×10^{-14}	6.3×10^{-14}
1000	4.7×10^{-13}	2.4×10^{-12}	6.1×10^{-14}	-
1050	8.7×10^{-13}	3.9×10^{-12}	7.2×10^{-14}	3.2×10^{-13}
1100	3.8×10^{-12}	1.9×10^{-11}	3.7×10^{-13}	1.4×10^{-12}

The k_p values of the Table 1 are plotted in an Arrhenius diagram shown in Figure 4 based on the diagram established by Brumm and Grabke for pure NiAl [39] corresponding to the grey crosses. The k_p values of the present work are one order of magnitude lower that those obtained with the "Particoat" slurry (slow) heat treatment [20]. This is because the high activity slurry process led to the formation of a top coat of hollow alumina spheres (slurry residues) on top of the aluminide coating. The metallic Al left in the residue contributed to the greater mass gain and the actual tortuous surface was not accurately assessed. In contrast, when the residue had been removed by sand blasting ("Particoat without foam"), the parabolic rate constants decreased by one order of magnitude [20] and are then similar to the k_p values of the fast aluminizing coatings of this work. The k_p values of the high activity pack aluminides were lower than ours over 1000°C but were of the same magnitude at 900 and 950°C [20]. In contrast, the high activity pack aluminides of Choux et al. [40, 41] on pure nickel oxidized faster at 900°C and similarly at 1000°C than our fast-aluminized coatings.

The main differences in the oxidation rates can be attributed to three major factors: internal defects, composition and microstructure. According to various works [25, 42], the internal defects appear to facilitate the rapid establishment of the protective alumina scales, which is in

line with our results, in particular at low temperatures (900°C). However, the increase of temperature could foster the outward diffusion of Ni to result in less protective scales ($NiAl_2O_4$) [43]. When considering composition, both our fast slurry aluminized and high activity pack aluminides from Choux et al. [40, 41] contain Ni_2Al_3 phase and are thus comparable but the absence of the internal defects in the pack aluminide resulted in the major growth of the non-protective θ-Al_2O_3. It is interesting to note that for an equivalent Ni_2Al_3 composition, the apparent rougher surface of the fast slurry coatings compared to the pack ones does not seem to contribute to an increase of the mass gain, hence to higher parabolic constants [44, 45]. One can thus hypothesize that the internal defects can indeed contribute to grow more protective oxide scales. The third major factor is microstructure, especially the grain size upon the first oxidation stages. Indeed, the grain size of the pack aluminides of Mollard et al. [20] were around twice (~50 µm) than our slurry ones (~20-25 µm). Therefore, the density of grain boundaries is greater in the slurry coatings, which increases the probability of high angle boundary responsible of faster alumina scale growth [46]. In order to confirm these hypotheses, the evolution of the oxide scales and of the coatings were characterized.

3.2.2 Characterization of the oxidized coatings

Raman spectroscopy was performed on the surface of the samples after the isothermal oxidation tests. Three spots were realized in different areas of surfaces: close to the centre, close to the edge and midway between the centre and edge.

Fig. 5 shows the Raman spectra (fluorescence domain) of the three regions probed on each surface of the samples. No major difference can be observed between each region (centre, middle or edge), which demonstrates the good homogeneity of the oxide layer grown. Unlike the slowly grown slurry aluminides of Mollard et al. [20], no signal was detected in the Raman domain, which is indicative of the absence of NiO and $NiAl_2O_4$. This difference may be explained by the greater Ni content (NiAl) in the slow slurry coatings than that of the fast

aluminide coatings (Ni_2Al_3 phase) of this work leading to the formation of Ni-containing oxide species after 100h of oxidation. Fig. 5 also shows the major formation of the metastable θ-Al_2O_3 at 900°C and the minor presence of the stable α-Al_2O_3. For higher temperatures, α-Al_2O_3 is the only detected oxide except at 950°C where tiny θ-Al_2O_3 peaks are still observed.

Figure 6 shows the XRD patterns of samples after the isothermal oxidation tests at different temperatures. The intensity of the characteristic peaks of α-Al_2O_3 progressively increases with oxidation temperature and the decrease of the aluminium content in the area probed by the X-rays is evidenced by the evolution of Ni_xAl_y phases as follows: Ni_2Al_3 (as-coated) → NiAl (as-coated, 900, 950 and 1000°C) → Ni_3Al (950, 1000 and 1050°C) → Ni(Al) at 1100°C. This evolution of the aluminium content can be explained by both the reaction with oxygen to form the oxide scale and by the inward Al and outward Ni diffusion increasing with temperature as demonstrated by the evolution of the nickel aluminide phases. An enlargement of the XRD patterns is observed for 900 and 950°C because the intensity of peaks is weak compared to the main NiAl phase. The main peaks obtained at the lowest temperature (900°C) in the enlarged area corresponds to the θ allotropic form as indexed in other works [36, 47-48]. A clear existence of this transition alumina lies in the observations of the SEM surfaces in Figure 7, with the typical needle-like morphology already reported by several authors [32-38]. As shown in Fig. 7.b, spallation of the oxide scale occurred in all samples very likely upon cooling as the TGA curves do not display any mass loss. Beneath the oxide scales, the voids observed result from preponderant cationic outward diffusion, as reported by Brumm and Grabke [49] and/or can be attributed to the non-reciprocal diffusion inducing a biaxial stress field perpendicular to the diffusion flux [50]. In contrast, the surfaces are fully covered with α-Al_2O_3 from 950°C onwards (Fig. 7c).

The cross-sections of the oxide scales formed after 100 h of oxidation in air at 900, 950, 1000 and 1100°C are shown in figure 8. The evolution of the average oxide scale thickness with the oxidation of temperature is gathered in Table 2.

Table 2: Average thickness of the oxide scales with the oxidation temperature

Temperature (°C)	900	950	1000	1050	1100
Oxide thickness (µm)	6.0 ± 0.9	0.9 ± 0.1	1.6 ± 0.2	3.4 ± 0.4	4.5 ± 0.4

The significant oxide thickness grown in the coatings oxidized at 900°C is in line with the TGA curves (Fig. 3a) and the SEM surface morphologies (Fig. 7) which suggested that the scale are thicker than the scales at 950 and 1000°C. Fig. 8a also demonstrates that the allotropic variety θ-Al_2O_3 presenting the characteristic whiskers grows over a very thin layer of α-Al_2O_3. This oxide scale is less compact compared to the α-Al_2O_3, which allows faster growth and explains the greater thickness at 900°C than the ones of the scales grown at higher temperatures even for a greater mass gain (e.g. 1050 and 1100°C) [47-48]. With increasing temperature, the scales become fully composed of α-Al_2O_3 and thicken. Moreover, the very thin layer observed at 950°C (~0.9 µm) (Fig. 8.b) is in line with the smaller mass gain recorded by the TGA upon the oxidation test (Fig. 3.a) and agrees with other works [32-35]. One can also note some tiny internal oxidation in the metal area close to the scale grown at 1100°C, which is consistent with the work of Brumm et al., who claimed that the internal oxidation could occur under defective alumina scales, in particular when the oxygen solubility increases in Ni_3Al and Ni after the transformation of NiAl [51].

Fig. 9 presents the SEM cross-sections of all oxidized samples etched with Kalling's n°2 reagent used to reveal the evolutions of microstructure. The composition of each layer was evaluated by making EDS spots before etching the cross-section (figure 10) and the results agree with the XRD patterns (fig. 6). However, the penetration of the X-rays was not deep

enough to detect the Ni_3Al sub-layer for the coating oxidized at 900°C. It can be observed that the two main layers of the coating before oxidation were still present after oxidation. The thickness of the outermost coating layer after oxidation is similar to the two main layers (~50µm) after coating and grain size is also about the same (~20±5 µm) after 100h of exposure at 900°C. By raising the oxidation temperature from 900 to 1000°C, the same coating layers are observed but the thickness of NiAl decreases while that of Ni_3Al increases as demonstrated by both the cross sections (fig. 9) and the EDS profiles (fig. 10). At 1050°C, NiAl has been fully consumed and only a layer of ~25 µm of Ni_3Al remains in contact with the oxide. After 100h of exposure at 1100°C, the EDS profile shows that between 17 and 19 at.% of aluminium remain in the subsurface (5 µm) of the substrate. This range seems to correspond at the critical aluminium content necessary to continue to form Al_2O_3. Indeed, Atas et al. [52] demonstrated that NiO is the main oxide produced after cyclic oxidation tests at 1000°C of a Ni-15Al bulk while a protective Al_2O_3 scale forms on Rene N5 coated by a Ni-19Al magnetron sputtering coating [53]. Figure 10 also clearly displays that the higher the oxidation temperature, the greater the Al flux towards the substrate. As such, the Al depletion in the first 50 microns falls to about 65% (900, 950 and 1000°C), 56% (1050°C) and 45% (1100°C) of the initial content. Yet, the interdiffusion in Ni_3Al and Ni(Al) is much lower than in NiAl [54]. One can thus anticipate that the overall Al reservoir to form exclusively Al_2O_3 will be maintained for extended periods of oxidation provided the alumina scale does not spall off as opposed to the slowly grown slurry coatings of Mollard et al. [20] that quickly lost the Al reservoir upon oxidation at the same temperatures.

Such evolution of these aluminium diffusion coatings with temperature is very well-known and it occurs because of the outward diffusion of Al to form the alumina scale and because of the significant compositional gradient between the Ni substrate and the Al-rich coating in the absence of any other alloying element to reduce the chemical activity of the diffusing species

[55]. This is particularly true in the initial transformation of Ni_2Al_3 into NiAl in line with the full transformation of the 240 µm-thick slurry Ni_2Al_3 coating in just 100h of oxidation at 1000°C reported by Wang et al. [56].

The typical plate-like microstructure of the martensitic transformations was only observed for the NiAl phase after the oxidation at 1000°C (fig. 8c) and was also identified by XRD with the characteristic peak of tetragonal $L1_0$-Ni_3Al phase. This martensitic transformation has been widely studied [57-61] and demonstrated to occur in Ni-rich NiAl phases provided the alloy contains less than ~35-37 at.% of Al, the coating has been exposed to temperatures at or above 1000°C and that fast cooling has been imposed to supress the $\beta \rightarrow \gamma'$ transformation [60]. In our work, the martensitic transformation is solely observed at 1000°C where the Al content is about 35 at%. In contrast, the Al content was already too low (<25 at%) or too high (> 37 at%) at, respectively, higher and lower temperatures (fig. 10). This statement is in line with the lack of martensitic transformation after 240h of isothermal oxidation at 1100°C of CVD aluminised Ni-based superalloy where the Al content appeared sufficiently high to maintain the NiAl phase. In contrast, the martensitic transformation occurred when the same coating was cyclically oxidized for 72h (3 cycles x24h) because the Al had dropped to about 31 at.% [62]. Despite such work could not clearly ascertain the origin of the undulations of the scale and underlying coating like the ones we observe in our fast aluminides (Fig. 8.c) under isothermal conditions, they may be related to the compressive stresses generated upon the growth of the oxide scale and the derived creep relaxation of the underlying coating [e.g. 63].

Nevertheless, the fast slurry aluminizing of this study generated a stable NiAl coating until 1000°C, like the pack-cemented ones, while the NiAl phase dissolved at only 950°C with the slow slurry aluminized coatings [20]. This result can be explained by both the greater amount of deposited slurry and the fastest heat treatment which produced coatings enriched in aluminium. Furthermore, the dissolution of the coating layers is more even than in the slowly-

grown slurry and pack cemented coatings, because no isolated islands of NiAl in Ni_3Al [29] have been observed. This implies that the rapid formation of the oxide scale from the Al-rich layer (Ni_2Al_3) and the absence of spallation upon the oxidation required less flux of Al through the coatings grain boundaries, in particular at the lowest oxidation temperatures. The precise origin of this may also be found in the potential defects (e.g. voids, dislocations, nanocavities) introduced upon this non-equilibrium aluminizing process, which deserves more thorough investigations by e.g. transmission electron microscopy in future works.

4 Conclusions

The isothermal oxidation behaviour of a fast slurry aluminized pure nickel substrate has been studied between 900 and 1100°C under synthetic air for 100h. The very short heat treatment applied ("flash" aluminizing) leads to the formation of a bi-layer coating composed by Ni_2Al_3 and NiAl with the former on top. The oxidation kinetics of the fast-aluminized coatings is similar to the slowly grown slurry and the pack-cemented ones and pure NiAl till 950°C. Above this temperature, the kinetics are one order of magnitude higher possibly because of the higher Al content of the flash coatings (Ni_2Al_3). In contrast, the coatings exclusively grow an α-Al_2O_3 alumina scale at temperatures above 1000°C and no other oxide was observed after 100h of oxidation even at 1100°C. Like with other aluminide coatings, the metastable alumina scale majorly forms at 900°C, which results in a thicker layer than those obtained at higher temperatures.

The degradation occurs evenly without forming diffusion islands by counter-current diffusion of Al and of Ni following the series: Ni_2Al_3 (as-coated) → NiAl (as-coated, 900°C, 950°C, 1000°C) → Ni_3Al (950°C, 1000°C, 1050°C) → Ni(Al) at 1100°C. Such even degradation and absence of Ni-containing oxides (e.g. $NiAl_2O_4$) may be due to high Al content, the smaller grains (hence greater density of grain boundaries) and potential introduction of internal defects through the non-equilibrium flash aluminizing. While the former has been experimentally demonstrated in this work, the internal defects have not, which opens an avenue of further investigation.

Authors' contributions

F. Pedraza and T. Kepa have designed the study. Both authors have contributed to the acquisition, analysis and interpretation of data, and have participated in drafting the article or revising it critically for important intellectual content. The three authors have made substantial contributions in the analysis and interpretation of data. Finally, all authors give final approval of the submitted version.

Acknowledgements

The authors gratefully acknowledge to the “Région Nouvelle Aquitaine” and Safran Aircraft Engines for partially funding this research.

References

[1] P. C Patnaik, Intermetallic coatings for high temperature application – a review, Mater. Manuf. Processes. 4 (1989) 133-152. doi: 10.1080/10426918908956276.

[2] J. R. Nicholls, Designing oxidation-resistant coating, JOM. 52 (2000) 28-35. doi: 10.1007/s11837-000-0112-2.

[3] B. M. Warnes, D. C. Punola, Clean diffusion coatings by chemical vapor deposition, Surf. Coating Technol. 94-95 (1997) 1-6. doi:10.1016/S0257-8972(97)00467-2.

[4] F. Pedraza, C. Tuohy, L. Whelan, A. D. Kennedy, High quality aluminide and thermal barrier coatings deposition for new and service exposed parts by CVD techniques, Mater. Sci. Forum. 461-464 (2004) 305-312. doi: 10.4028/www.scientific.net/MSF.461-464.305.

[5] S. C. Kung, R. A. Rapp, Kinetic study of aluminization of iron by using the pack cementation technique, J. Electrochem. Soc. 135 (1988) 731-741. doi: 10.1149/1.2095732.

[6] L. Levin, A. Ginzburg, L. Klinger, T. Werber, A. Katsman, P. Schaaf, Controlled formation of surface layers by pack aluminization, Surf. Coating Technol. 106 (1998) 209-213. doi: 10.1016/S0257-8972(98)00529-5.

[7] H. Glasbrenner, O. Wedemeyer, Comparison of hot dip aluminised F82H-mod. steel after different subsequent heat treatments, J. Nucl. Mater. 257 (1998) 274-281. doi: 10.1016/S0022-3115(98)00456-5.

[8] J. Chen, G. Z. Dai, J. W. Zhao, X. M. Huang, J. Han, Optimization of process parameters of hot-dip aluminized coating, Adv. Mater. Research. 391-392 (2011) 46-50. doi: 10.4028/www.scientific.net/AMR.391-392.46.

[9] F. Bozza, G. Bolelli, C. Giolli, A. Giorgetti, L. Lusvarghi, P. Sassatelli, A. Scrivani, A. Candeli, M. Thoma, Diffusion mechanisms and microstructure development in pack aluminizing of Ni-based alloys, Surf. Coating Technol. 239 (2014) 147-159. doi: 10.1016/j.surfcoat.2013.11.034.

[10] G. W. Goward, D. H. Boone, Mechanisms of formation of diffusion aluminide coatings on nickel-base superalloys, Oxid. Met. 3 (1971) 475-495. doi: 10.1007/BF00604047.

[11] A. J. Rasmussen, A. Agüero, M. Gutierrez, M. José Landeira Østergård, Microstructures of thin and thick slurry aluminide coatings on Inconel 690, Surf. Coating Technol. 202 (2008) 1479-1485. doi: 10.1016/j.surfcoat.2007.06.056.

[12] M. C. Galetz, X. Montero, M. Mollard, M. Günthner, F. Pedraza, M. Schütze, The role of combustion synthesis in the formation of slurry aluminization, Intermetallics. 44 (2014) 8-17. doi: 10.1016/j.intermet.2013.08.002.

[13] L. Čelko, S. Hutarova, M. Petrenec, K. Obrtlik, M. Hrckova, et T. Podrabsky, Microstructural characterization of slurry aluminide diffusion coatings, Mater. Sci. Forum 782 (2014) 584-589. doi: 10.4028/www.scientific.net/MSF.782.584.

[14] F. Pedraza, M. Mollard, B. Rannou, J. Balmain, B. Bouchaud, G. Bonnet, Potential thermal barrier coating systems from Al microparticles. Mechanisms of coating formation on pure nickel, Mater. Chem. Phys. 134 (2012) 700-705. doi: 10.1016/j.matchemphys.2012.03.053.

[15] G. Bonnet, M. Mollard, B. Rannou, J.Balmain, F. Pedraza, X. Montero, M. Galetz, M. Schütze, Initial aluminizing steps of pure nickel from Al micro-particles, Defect Diffus. Forum 323-325 (2012) 381-386. doi: 10.4028/www.scientific.net/DDF.323-325.381.

[16] F. Pedraza, M. Mollard, B. Rannou, B. Bouchaud, J. Balmain, G. Bonnet, Oxidation resistance of thermal barrier coatings based on hollow alumina particles, Oxid. Met. 85 (2016) 231-244. doi: 10.1007/s11085-015-9570-3.

[17] J. T. Bauer, X. Montero, M. C. Galetz, Fast heat treatment methods for al slurry diffusion coatings on alloy 800 prepared in air, Surf. Coating Technol. 381 (2020) 125140. doi: 10.1016/j.surfcoat.2019.125140.

[18] T. Kepa, F. Pedraza, F. Rouillard, Intermetallic formation of Al-Fe and Al-Ni phases by ultrafast slurry aluminization (flash aluminizing), Surf. Coating Technol. 397 (2020) 126011. doi: 10.1016/j.surfcoat.2020.126011.

[19] B.A. Pint, The role of chemical composition on the oxidation performance of aluminide coatings. Surf. Coating Technol. 188–189 (2004) 71– 78. doi: 10.1016/j.surfcoat.2004.08.007

[20] M. Mollard, B. Rannou, B. Bouchaud, J. Balmain, G. Bonnet, F. Pedraza, Comparative degradation of nickel aluminized by slurry and by pack cementation under isothermal

conditions, Corros. Sci. 66 (2013) 118-124. doi: 10.1016/j.corsci.2012.09.009.

[21] B. Rannou, B. Bouchaud, J. Balmain, G. Bonnet, F. Pedraza, Comparative isothermal oxidation behaviour of new aluminide coatings from slurries containing Al particles and conventional out-of-pack aluminide coatings, Oxid. Met. 81 (2014) 139-149. doi: 10.1007/s11085-013-9427-6.

[22] M. C. Galetz, C. Oskay, S. Madloch, Microstructural degradation and interdiffusion behavior of NiAl and Ge-modified NiAl coatings deposited on Alloy 602 CA, Surf. Coating Technol. 364 (2019) 211-217. doi: 10.1016/j.surfcoat.2019.02.048.

[23] A. Littner, F. Pedraza, A.D Kennedy, P. Moretto, L. Peich, T. Weber, M. Schütze, Performance and Thermal Stability of Pt-modified Al-diffusion Coatings for Superalloys under Cyclic and Isothermal Conditions. Mater. at High Temp. 22 (2005) 411-420. doi: 10.1179/mht.2005.048.

[24] C. Curfs, X. Turrillas, G. B. M. Vaughan, A. E. Terry, Å. Kvick, M. A. Rodríguez, Al–Ni intermetallics obtained by SHS; A time-resolved X-ray diffraction study, Intermetallics. 15 (2007) 1163-1171. doi: 10.1016/j.intermet.2007.02.007.

[25] M. Shen, Y. Gu, P. Zhao, S. Zhu, F. Wang, Synthesis of advanced aluminide intermetallic coatings by low-energy Al-ion radiation, Scientific Reports. 6 (2016) 26535. doi: 10.1038/srep26535.

[26] Q. Fan, H. Chai, Z. Jin, Dissolution–precipitation mechanism of self-propagating high-temperature synthesis of mononickel aluminide, Intermetallics. 9 (2001) 609–619. doi: 10.1016/S0966-9795(01)00046-2.

[27] Y. Liu, X. Fan, M. Zhang, X. Qin, Chemical reaction of in situ processing of $NiAl/Al_2O_3$ composite by using thermite reaction, Journal of Wuhan University of Technology. 20 (2005) 90-92+119.

[28] H-E. Schaefer, F. Baier, M. A. Müller, K.J. Reichl, K. Reimann, A.A. Rempel, K. Sato, F. Ye, X. Zhang, W. Sprengel, Vacancies and atomic processes in intermetallics - from crystals to quasicrystals and bulk metallic glasses: vacancies and atomic processes in intermetallics, Phys. Status Solidi B. 248 (2011) 2290-2299. doi: 10.1002/pssb.201147103.

[29] A. Agüero, K. Spiradek, S. Höfinger, M. Gutiérrez, R. Muelas, Microstructural evolution of slurry Fe aluminide coatings during high temperature steam oxidation, Mater. Sci. Forum. 595-598 (2008) 251-259. doi: 10.4028/www.scientific.net/MSF.595-598.251.

[30] C. Boulesteix, F. Pedraza, Characterisation of aluminium diffusion coatings elaborated on austenitic stainless steels and on ferritic-martensitic steels, Surf. Coating Technol. 339 (2018) 27-36. doi: 10.1016/j.surfcoat.2018.01.086.

[31] H. Okamoto, Al-Ni (aluminium-nickel), J Phase Equilib. Diffus. 25 (2004) 394. doi: 10.1361/15477030420232 1547-7037.

[32] G. C. Rybicki, J. L. Smialek, Effect of the θ-α-Al_2O_3 transformation on the oxidation behaviour of β-NiAl + Zr, Oxid. Met. 31 (1989) 275-304. doi: 10.1007/BF00846690.

[33] H. J. Grabke, Oxidation of NiAl and FeAl, Intermetallics, 7 (1999) 1153-1158. doi: 10.1016/S0966-9795(99)00037-0.

[34] V. K. Tolpygo, D. R. Clarke, Microstructural study of the theta-alpha transformation in alumina scales formed on nickel-aluminides, Mater. at High Temp. 17 (2000) 59-70. doi: 10.1179/mht.2000.011.

[35] H. El Kadiri, R. Mollins, Y. Bienvenu, M. F. Horstemeyer, Abnormal high growth rates of metastable aluminas on FeCrAl alloys, Oxid. Met. 64 (2005) 63-97. doi: 10.1007/s11085-005-5715-0.

[36] V. Kolarik, M. del M. Juez-Lorenzo, H. Fietzek, Oxidation of micro-sized spherical aluminium particles, Mater. Sci. Forum. 696 (2011) 290-295. https://www.scientific.net/MSF.696.290.

[37] F. Velasco, S. Guzmán, C. Moral, A. Bautista, Oxidation of micro-sized aluminium particles: hollow alumina spheres, Oxid. Met. 80 (2013) 403-422. doi: 10.1007/s11085-013-9408-9.

[38] M. Mollard, Elaboration de systèmes barrière thermique par barbotine: comportement du nickel et de ses superalliages revêtus en oxydation cyclique à haute température, PhD Thesis, La Rochelle University (in French) (2012).

[39] M. W. Brumm, H. J. Grabke, The oxidation behaviour of NiAl-I. Phase transformations in the alumina scale during oxidation of NiAl and NiAl-Cr alloys, Corros. Sci. 33 (1992) 1677-1690. doi: 10.1016/0010-938X(92)90002-K.

[40] C. Choux, A. J. Kulińska, S. Chevalier, High temperature reactivity of nickel aluminide diffusion coatings, Intermetallics. 16 (2008) 1-9. doi: 10.1016/j.intermet.2007.07.014.

[41] C. Choux, Elaboration et réactivité à haute température de revêtements d'intermétalliques, application aux atmosphères complexes, PhD Thesis, Burgundy University (in French) (2008).

[42] A. Y. Lozovoi, A. Alavi, M. W. Finnis, Surface stoichiometry and the initial oxidation of NiAl(110), Physical Review Letters. 85 (2000) 610-613. doi: 10.1103/PhysRevLett.85.610.

[43] F. Pedraza B. Bouchaud, Solid state interfacial reactions in a ceria-coated Ni-based superalloy, Surf. Coating Technol. 383 (2020) 125202. doi: 10.1016/j.surfcoat.2019.125202.

[44] C. Piehl, Zs. Toekei, H. J. Grabke, Influence of chromium diffusion and different surface finishes on the oxidation behaviour of chromium steels, Mater. High. Temp. 17 (2000) 243-246. doi: 10.1179/mht.2000.17.2.010.

[45] A. M. Huntz, B. Lefevre, F. Cassino, Roughness and oxidation: application to NiO growth on Ni at 800°C, Mater. Sci. Eng, A. 290 (2000) 190-197. doi: 10.1016/S0921-5093(00)00944-8.

[46] J. K. Doychak, The evolution and growth of Al_2O_3 scales on β-NiAl, PhD Thesis, Case Western Reserve University, Cleveland, Ohio (1986). NASA CR-175097.

[47] R. S. Zhou, R. L. Snyder, Structures and transformation mechanisms of the η, γ and θ transition aluminas, Acta Cryst. (1991) 617-630. doi: 10.1107/S0108768191002719.

[48] J. S. Lee, H. S. Kim, N. Park, T. J. Lee, M. Kang, Low temperature synthesis of α-alumina from aluminum hydroxide hydrothermally synthesized using $[Al(C_2O_4)_x(OH)_y]$ complexes, Chem. Eng. J. 230 (2013) 351-360. doi: 10.1016/j.cej.2013.06.099.

[49] M. W. Brumm, H. J. Grabke, Oxidation behaviour of NiAl-II Cavity formation beneath the oxide scale on NiAl of different stoichiometries. Corros. Sci. 34 (1993) 547-561. doi: 10.1016/0010-938X(93)90271-H.

[50] Z. Suo, D. V. Kubair, A. G. Evans, D. R. Clarke, V. K. Tolpygo, Stresses induced in alloys by selective oxidation. Acta Mater. 51 (2003) 959-974. doi:10.1016/S1359-

6454(02)00499-8.

[51] M. W. Brumm, H. J. Grabke, B. Wagemann, The oxidation of NiAl-III. Internal and intergranular oxidation, Corros. Sci. 36 (1994) 37-53. doi: 10.1016/0010-938X(94)90107-4.

[52] M. S. Atas, M. Yildirim, J Alloys Compd. Temporal evolution, coarsening behavior and oxidation resistance of Ni–15Al superalloy, 809 (2019) 151784. doi: 10.1016/j.jallcom.2019.151784.

[53] H. Yao, L. Yang, Z. Bao, S. Zhu, F. Wang, Low inter-diffusivity γ'-base bondcoats for single crystal superalloy René N5 I Primary study of microstructures and oxidation behaviors at 1100 ºC, Corros. Sci. 147 (2019) 299-312. doi: 10.1016/j.corsci.2018.11.021.

[54] J. M. Brossard, B. Panicaud, J. Balmain, G. Bonnet, Modelling of aluminized coating growth on nickel, Acta Mater 55 (2007) 6586-6595. doi: 10.1016/j.actamat.2007.08.025.

[55] R. Yang, Y. Wu, Q. Wu, S. Li, Y. Ma, S. Gong, Microstructure and oxidation behavior of modified aluminide coating on Ni_3Al-based single crystal superalloy, Chinese J. Aeronaut. 25 (2012) 825-830. doi: 10.1016/S1000-9361(11)60451-2.

[56] H. Wang, Y. Zhang, J. Cheng, Y. Li, High temperature oxidation resistance and microstructure change of aluminized coating on copper substrate, Transactions of Nonferrous Metals Society of China. 25 (2015) 184-190. doi: 10.1016/S1003-6326(15)63594-4.

[57] S. Rosen, J. A. Goebel, Trans. TMS-AIME 242 (1968) 722.

[58] J. L. Smialek, Martensite in NiAl oxidation-resistant coatings, Metall. Trans. 2 (1971) 913-915. doi: 10.1007/BF02662758.

[59] J. L. Smialek, R. F. Hehemann, Transformation Temperatures of Martensite in β-Phase Nickel Aluminide, Metall. Trans. 4 (1973) 1571-1575. doi: 10.1007/BF02668010.

[60] Y. Zhang, J. A. Haynes, B. A. Pint, I. G. Wright, W. Y. Lee, Martensitic transformation in CVD NiAl and (Ni,Pt)Al bond coatings, Surf. Coating. Technol. 163-164 (2003) 19-24. doi: 10.1016/S0257-8972(02)00585-6.

[61] S. V. Kositsyn, A. I. Valiullin, N. V. Kataeva, I. I. Kositsyna, Investigation of microcrystalline NiAl-based alloys with high-temperature thermoelastic martensitic

transformation: I. Resistometry of the Ni-Al and Ni-Al-X (X = Co, Si, or Cr) alloys, Phys. Met. Metall. 102 (2006) 391-405. doi: 10.1134/S0031918X06100073.

[62] B. Bouchaud, J. Balmain, F. Pedraza, Cyclic and isothermal xidation at 1,100 °C of a CVD aluminised directionally solidified Ni superalloy, Oxid. Met. 69 (2008) 193-210. doi: 10.1007/s11085-008-9092-3.

[63] V.K. Tolpygo, D.R. Clarke, On the rumpling mechanism in nickel-aluminide coatings Part I: an experimental assessment. Acta. Mater. 52 (2004) 5115-5127. doi: 10.1016/S1359-6454(04)00428-8.

List of figure captions

Figure 1: (a) Etched (Kalling n°2) SEM cross-section of the as-aluminized Ni substrate and (b) Al composition (at.%) across the coating.

Figure 2: XRD patterns of the as-coated samples before oxidation.

Figure 3: (a) TGA curves of the fast aluminized nickel oxidized for 100h in air at different temperatures and (b) the corresponding $(\Delta M/S)^2 = f(t)$ curves.

Figure 4: Arrhenius diagrams of $\log(k_p)$ *vs.* 1/T for the high activity aluminide coatings fabricated by slurry [this work, 20] and pack cementation [20, 39-41].

Figure 5: Raman spectra (fluorescence domain) of the fast-aluminized nickel samples after 100h of isothermal oxidation at different temperatures in air.

Figure 6: XRD patterns of the fast-aluminized nickel samples after 100h of isothermal oxidation at different temperatures in air. (An enlargement is added to show the theta alumina; crosses represent unidentified compounds).

Figure 7: SEM surface morphology of the fast-aluminized samples oxidized in air for 100h at 900°C (a: secondary electrons; b: back-scattered electrons) and at 950°C (c: secondary electrons).

Figure 8: SEM cross-sections of oxide scale formed on the fast-aluminized nickel samples after 100h of isothermal oxidation at (a) 900°C, (b) 950°C, (c) 1000°C, (d) 1100°C. A Ni electroplate layer was deposited for metallographic purposes.

Figure 9: Etched SEM cross-sections of oxidized nickel coatings for 100h at (a) 900°C, (b) 950°C, (c) 1000°C, (d) 1050°C and (e) 1100°C.

Figure 10: EDS composition profiles of oxidized nickel coatings for 100h for different temperatures.

Figures

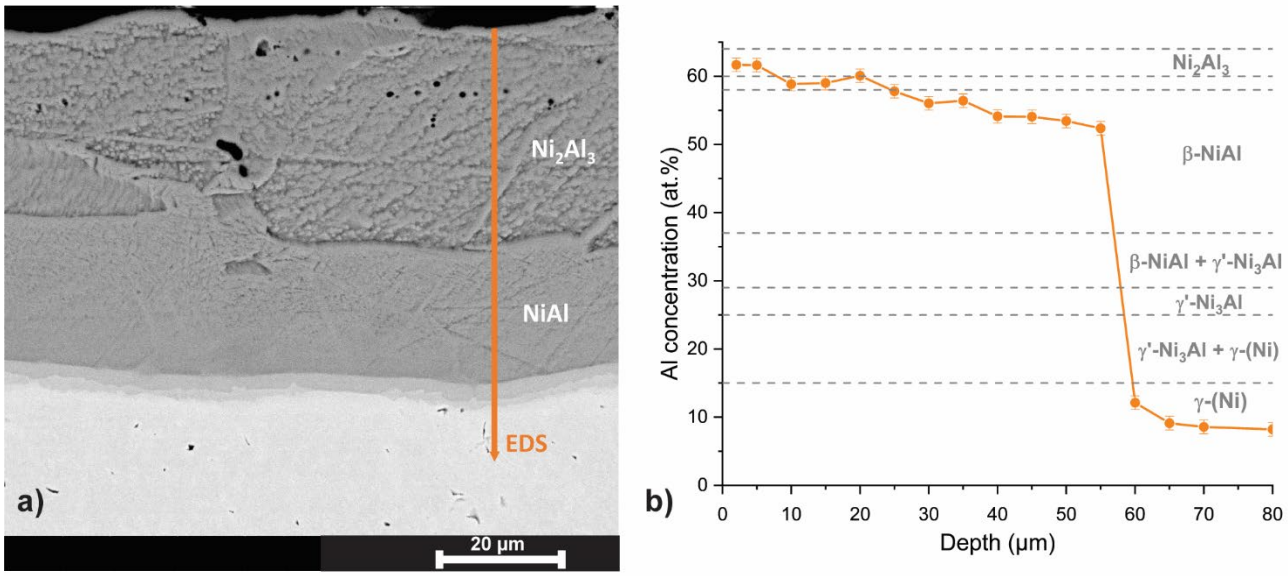

Fig. 1

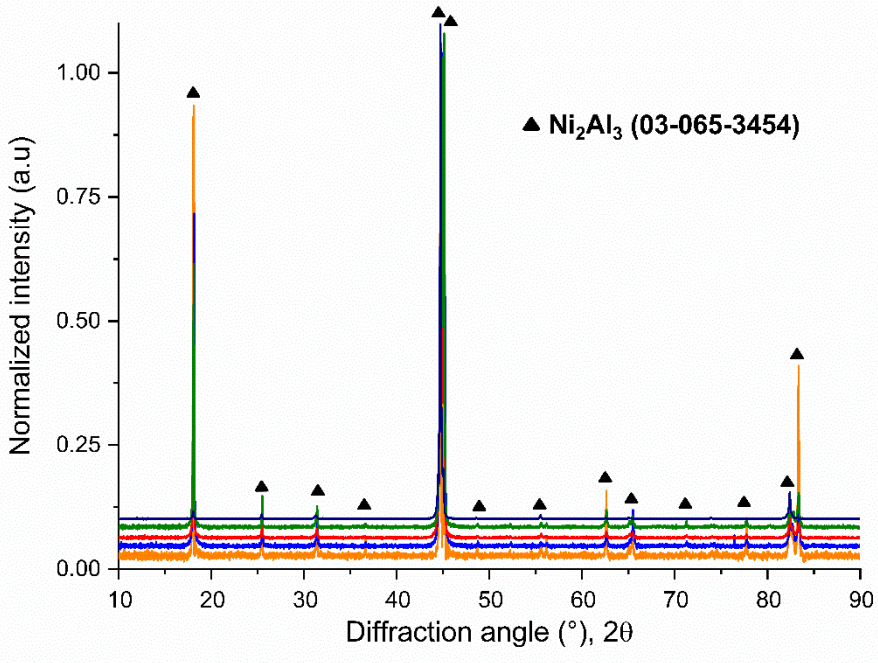

Fig. 2

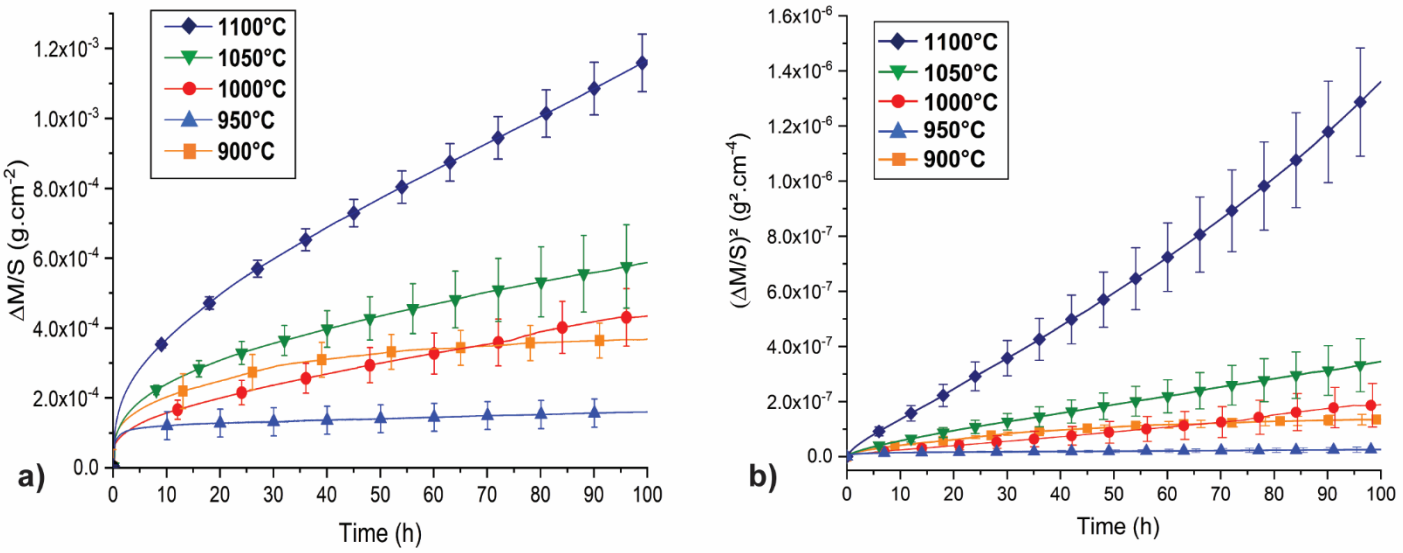
a)
b)
1100°C
1050°C
1000°C
950°C
900°C
ΔM/S (g.cm-2)
(ΔM/S)² (g².cm-4)
Time (h)
Time (h)

Fig. 3

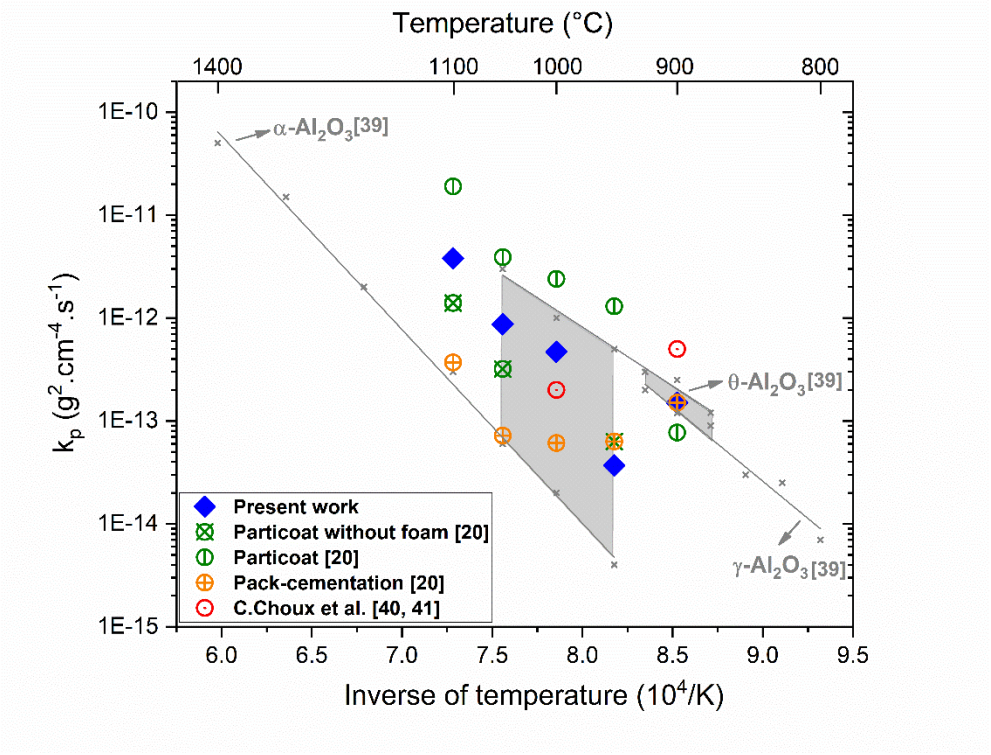
Temperature (°C)
1400
1100
1000
900
800
α-Al2O3[39]
θ-Al2O3[39]
γ-Al2O3[39]
Present work
Particoat without foam [20]
Particoat [20]
Pack-cementation [20]
C.Choux et al. [40, 41]
kp (g2.cm-4.s-1)
Inverse of temperature (10⁴/K)

Fig. 4

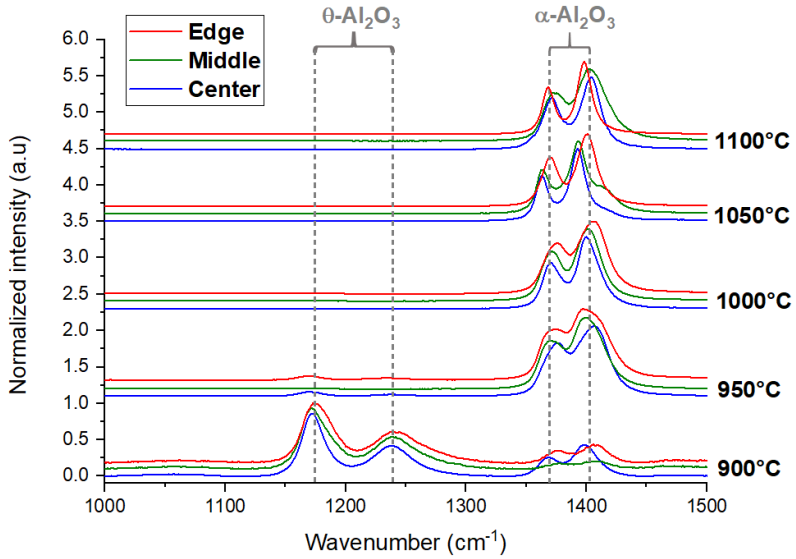
θ-Al2O3
α-Al2O3
Edge
Middle
Center
1100°C
1050°C
1000°C
950°C
900°C
Normalized intensity (a.u)
Wavenumber (cm-1)

Fig. 5

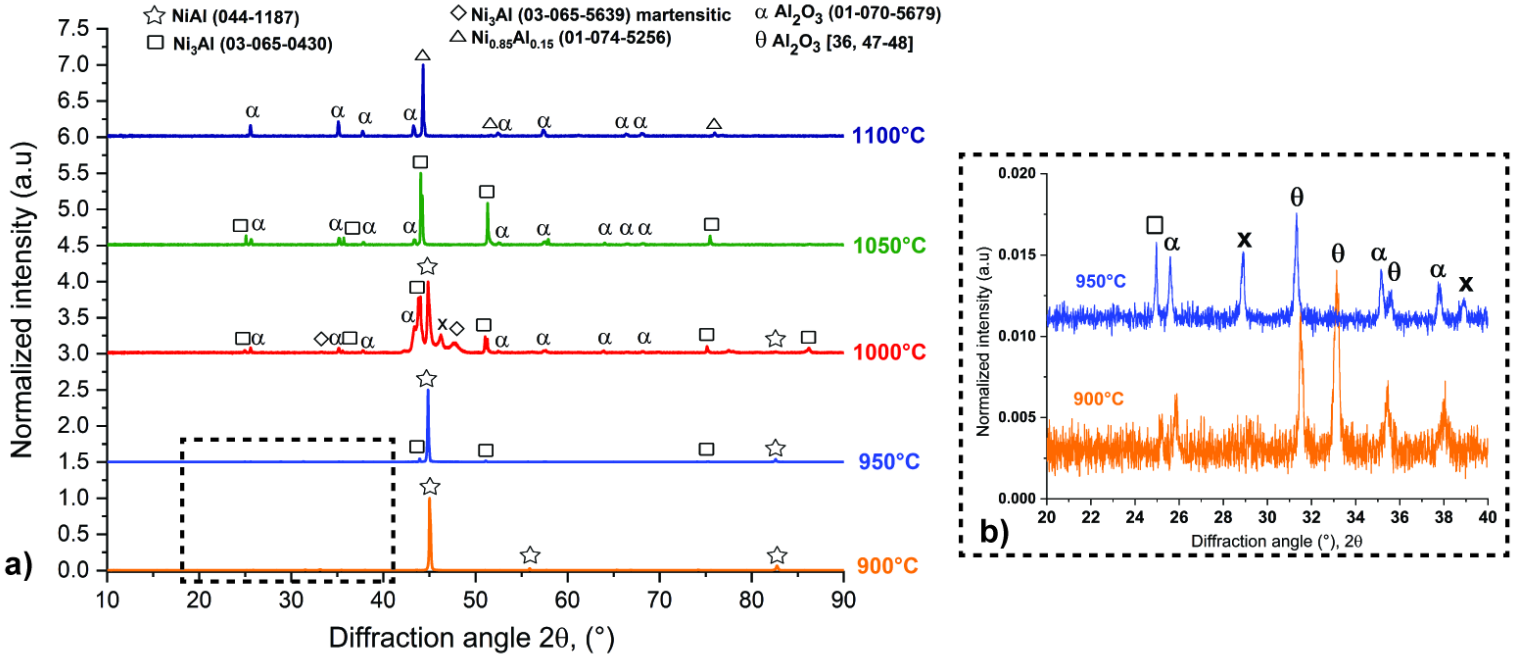
NiAl (044-1187)
Ni3Al (03-065-0430)
Ni3Al (03-065-5639) martensitic
Ni0.85Al0.15 (01-074-5256)
α Al2O3 (01-070-5679)
θ Al2O3 [36, 47-48]
1100°C
1050°C
1000°C
950°C
900°C
Normalized intensity (a.u)
Diffraction angle 2θ, (°)
a)
b)
Diffraction angle (°), 2θ

Fig. 6

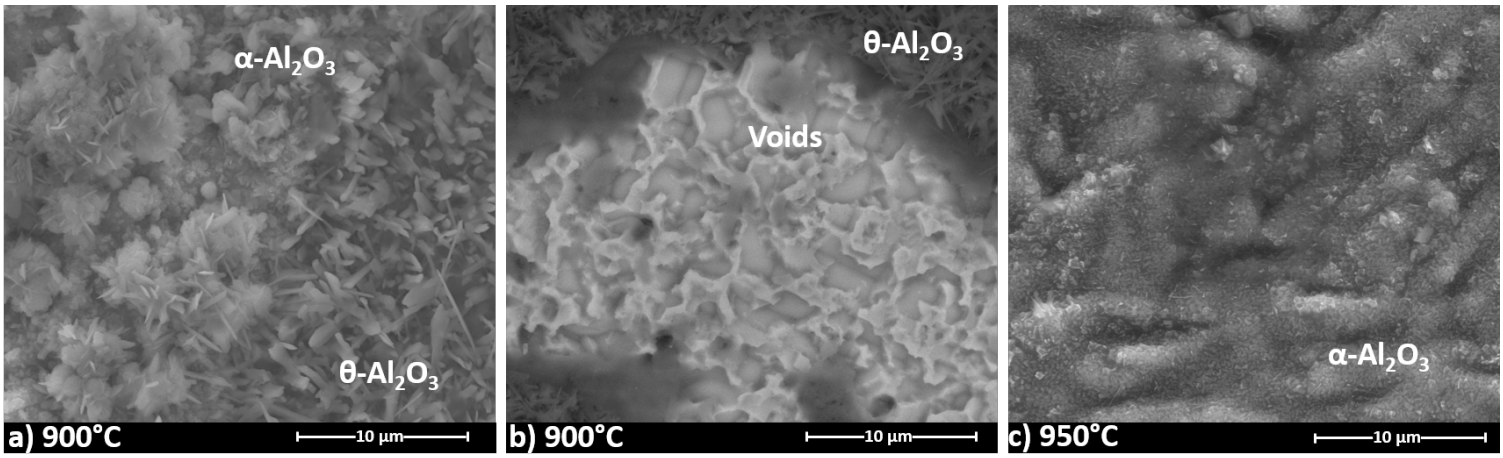
α-Al2O3
θ-Al2O3
a) 900°C
10 µm
θ-Al2O3
Voids
b) 900°C
10 µm
α-Al2O3
c) 950°C
10 µm

Fig. 7

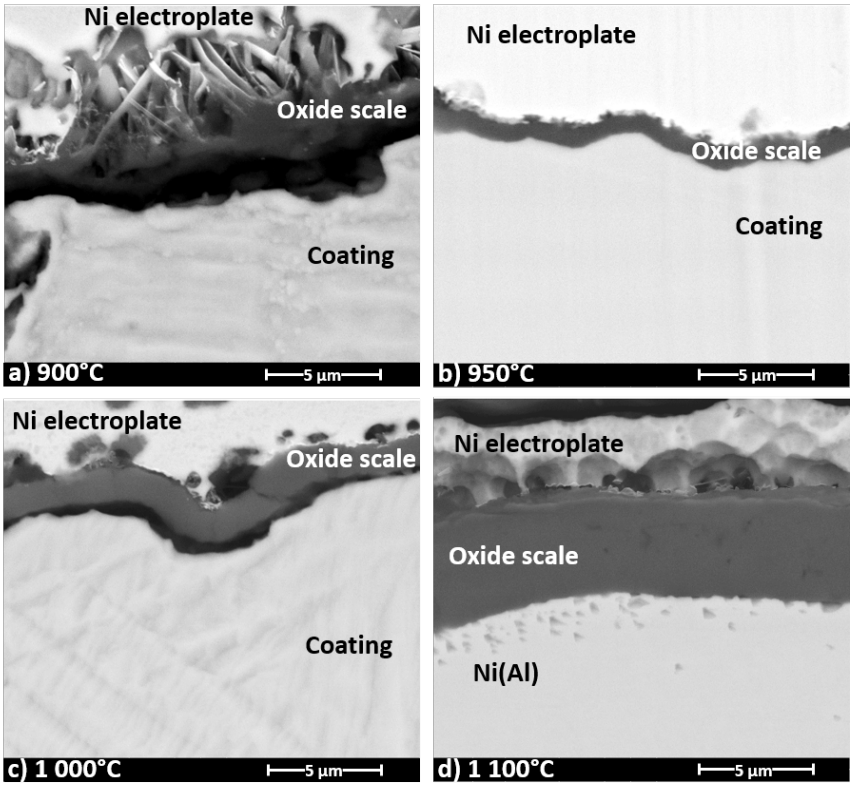
Ni electroplate
Oxide scale
Coating
a) 900°C
5 µm
Ni electroplate
Oxide scale
Coating
b) 950°C
5 µm
Ni electroplate
Oxide scale
Coating
c) 1 000°C
5 µm
Ni electroplate
Oxide scale
Ni(Al)
d) 1 100°C
5 µm

Fig. 8

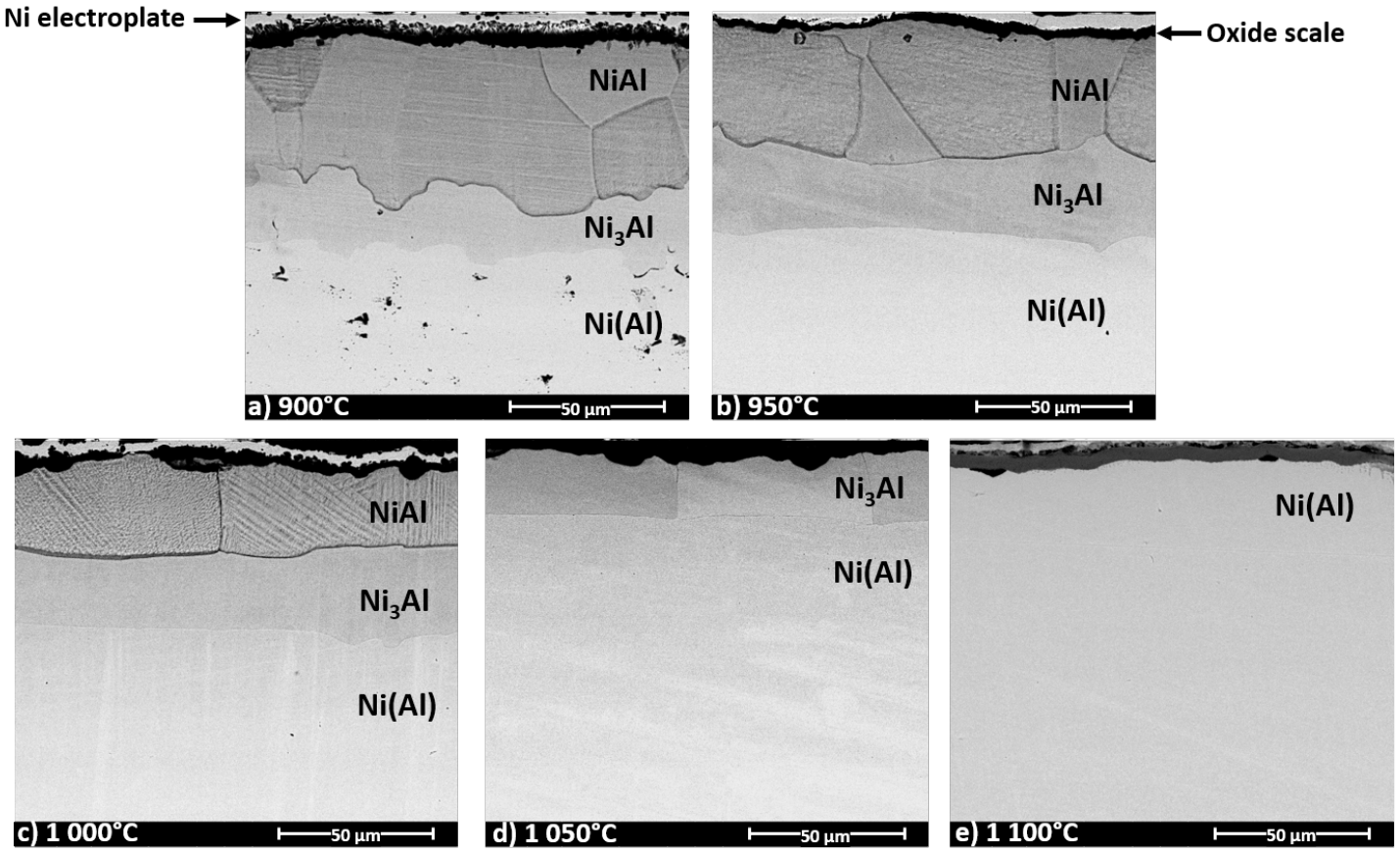
Ni electroplate
Oxide scale
NiAl
Ni3Al
Ni(Al)
a) 900°C
b) 950°C
c) 1 000°C
d) 1 050°C
e) 1 100°C
50 µm

Fig. 9

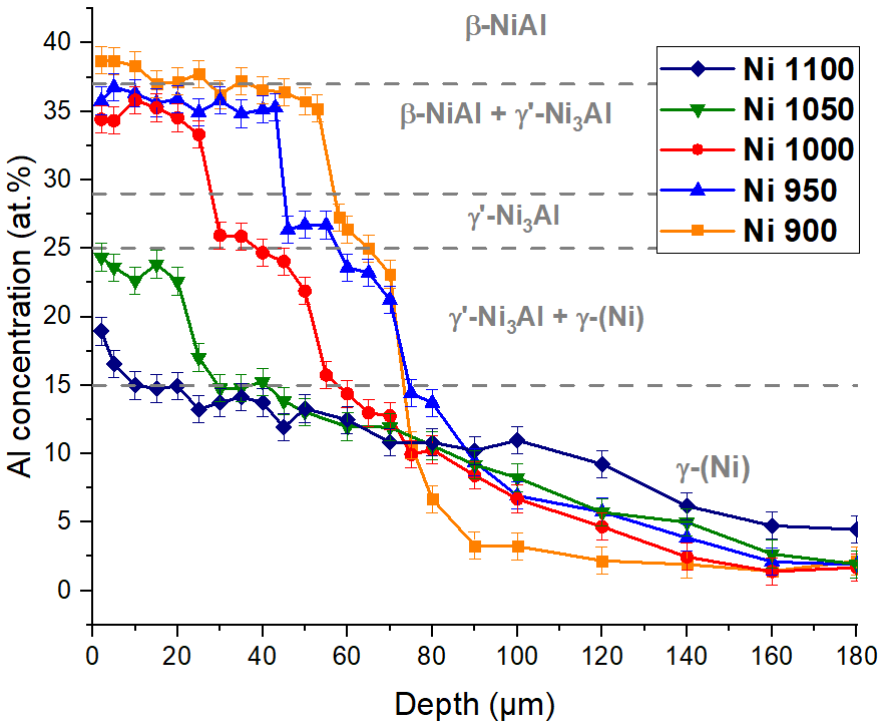
β-NiAl
β-NiAl + γ'-Ni3Al
γ'-Ni3Al
γ'-Ni3Al + γ-(Ni)
γ-(Ni)
Ni 1100
Ni 1050
Ni 1000
Ni 950
Ni 900
Al concentration (at.%)
Depth (µm)
0
5
10
15
20
25
30
35
40
0
20
40
60
80
100
120
140
160
180

Fig. 10